

UC Davis

UC Davis Previously Published Works

Title

Ultra-high resolution adaptive optics: optical coherence tomography for in vivo imaging of healthy and diseased retinal structures

Permalink

<https://escholarship.org/uc/item/4kj3d6h9>

ISBN

978-0-8194-7019-5

Authors

Zawadzki, Robert J
Zhang, Yan
Jones, Steven M
et al.

Publication Date

2008-02-07

DOI

10.1117/12.764115

Peer reviewed

Ultra-high resolution adaptive optics - optical coherence tomography for in vivo imaging of healthy and diseased retinal structures

Robert J. Zawadzki¹, Yan Zhang², Steven M. Jones³, Stacey S. Choi¹, Barry Cense²,
Julia W. Evans^{1,3}, Donald T. Miller², Scot S. Olivier³ and John S. Werner¹

¹ Vision Science and Advanced Retinal Imaging Laboratory (VSRI) and Dept. of Ophthalmology & Vision Science, University of California Davis, 4860 Y Street, Suite 2400, Sacramento, CA 95817

² School of Optometry, Indiana University, 800 E. Atwater Ave., Bloomington, IN 47405

³ Lawrence Livermore National Laboratory, 6000 East Avenue, Livermore, CA 94550

ABSTRACT

Ultra-high isotropic resolution imaging of retinal structures was made possible with an adaptive optics system using dual deformable mirrors and a Fourier-domain optical coherence tomography (Fd-OCT) system with correction for longitudinal chromatic aberration. This system was used to image microscopic retinal structures of healthy as well as diseased retinas in vivo. The improved resolution and contrast enhanced visualization of morphological structures in the retina can be clearly seen. The benefits of this instrument are apparent from comparison of new images with those acquired using a previous generation AO-OCT instrument. Big change in the appearance of speckle field (reduction in speckle size) can be observed as well. Additionally, further improvements in volumetric data acquisition and image representation will be discussed. This includes creation of large Field of View (FOV) AO-OCT volume from multiple sub-volumes and its visualization. Also techniques and results of reducing speckle contrast by averaging multiple B-scans will be presented.

Keywords: (110.4500) Optical coherence tomography; (010.1080) Adaptive optics; (170.0110) imaging system; (120.3890) Medical optics instrumentation; (170.4470) ophthalmology; (220.1000) Aberration compensation

1. INTRODUCTION

In recent years Adaptive optics - optical coherence tomography (AO-OCT) [1-8] has realized an improvement in lateral resolution compared to stand alone Fd-OCT [9-11]. We previously reported [12] an ultra-high resolution (UHR) OCT that is capable of real-time imaging with high volumetric resolution ($\sim 3 \mu\text{m}$ in all three dimensions). Its basic components have been described previously which include Fourier-domain OCT (Fd-OCT) with correction for longitudinal chromatic aberration (done by achromatizing lens) and AO allowing monochromatic aberration correction using two deformable mirrors (DM's). In this paper we report results on using this instrument for in-vivo imaging of healthy and diseased retinal structures. New ways of improving system feasibility for clinical studies are presented including creation of large Field of View (FoV) AO-OCT volumes constructed from multiple smaller volumes and co-registration of these large AO-OCT volumes to fundus photos. Additionally, impact of the speckle contrast, one of the inherent built-in problems in OCT coherent detection scheme, will be discussed. As previously noted by other investigators in order to reduce this speckle noise we decided to acquire multiple B-scans (over the same location) and register them and then create an average intensity image (each pixel value is calculated as an average intensity from all frames). Several results of implementing this method in imaging diseased retina will also be presented.

2. MATERIALS AND METHODS

The AO-OCT system used in this paper has already been described in detail elsewhere [12]. A brief overview of the system is provided, followed by description of our volumetric data manipulation software and speckle reduction method.

*email rjzawadzki@ucdavis.edu; phone 1 916 734-5839; fax 1 916 734-4543; <http://vsri.ucdavis.edu/>

Ophthalmic Technologies XVIII, edited by Fabrice Manns, Per G. Söderberg, Arthur Ho, Bruce E. Stuck, Michael Belkin, Proc. of SPIE Vol. 6844, 684408, (2008) · 1605-7422/08/\$18 · doi: 10.1117/12.764115

2.1. Experimental system

Figure 1. shows a very basic schematic of generic AO-OCT system that consist of Michelson interferometer with built in Adaptive Optics system (with wavefront corrector and wavefront sensor) in its sample arm.

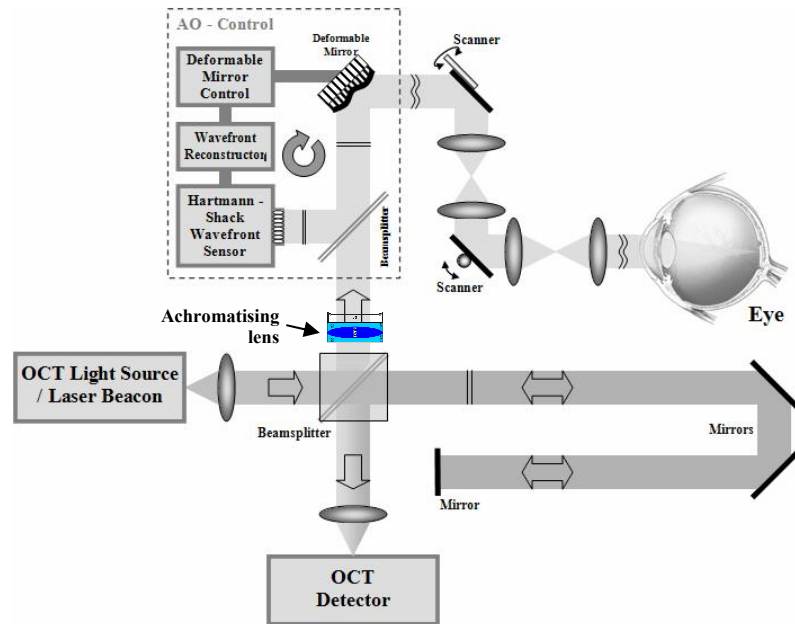


Fig. 1: Simplified schematic of Michelson Interferometer based AO-OCT instrument.

Please note position of achromatizing lens on Fig.1., at the beginning of the sample arm. Importance of chromatic aberration correction in UHR AO-OCT imaging has been theoretical and experimentally demonstrated by Fernández et al [13-15]. This lens cancels longitudinal chromatic aberrations of the human eye and therefore allows high lateral resolution imaging with polychromatic light with large pupil diameters. The actual AO-OCT system developed in our laboratory occupies a 5 ft x 6 ft laboratory optical table. In the optical design, we used a cascade of focal telescopes (created by pairs of spherical mirrors instead of lenses) to produce conjugate planes of the eye pupil with all key optical components, including X and Y scanning mirrors, two wavefront correctors and a Hartmann-Shack (H-S) wavefront sensor (which uses the OCT imaging light for wavefront reconstruction). The detection channel of the OCT system consists of a custom-design spectrometer allowing 2 mm axial scanning depth in the eye. Fd-OCT data acquisition software developed by Bioptigen Inc. Durham, NC processes displays and streams AO-OCT B-scan data to system memory in real time simultaneously. The light source for both OCT and AO subsystems is an SLD Broadlighter T840-HP (836@112nm; Pout = 16 mW) from Superlum LTD, allowing 3 μ m axial resolution in the retina. Spectra and axial PSF of this light source is shown below.

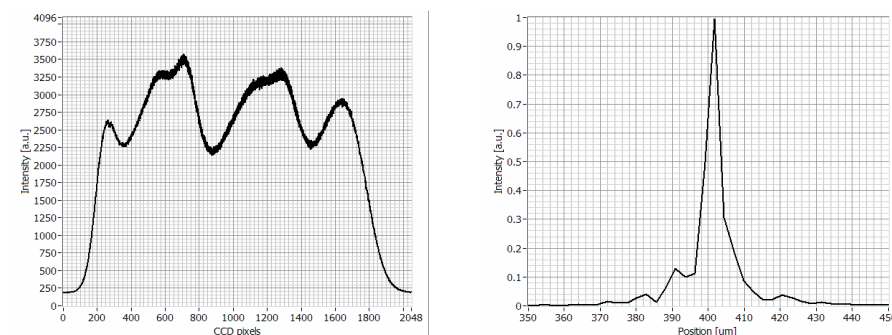


Fig. 2. Left: Spectra of the SLD: T840-HP acquired by the OCT detection spectrometer. Right: corresponding PSF.

Separate PC controls the AO subsystem of our instrument for measuring wavefront aberrations of the eye and drives both deformable mirrors (one at a time) in a closed loop. In our AO sub-system we used two wavefront correctors: a 37 actuator Bimorph Deformable Mirror (DM1) from AOptix and a 144 actuator MEMS Deformable Mirror (DM2) manufactured by Boston Micromachines. The AO system uses the bimorph DM for low-order aberration correction (defocus and astigmatism) eliminating the need for trial lenses to correct individual subject's refractive errors up to ± 3 diopters of defocus. The same mirror is also used to shift the focus of the AO-OCT beam axially onto retinal structures of interest. Our AO sub-system allows archiving of H-S wavefront centroid displacements and RMS error. This can be used as a measure of the wavefront correction and time-linked to the corresponding OCT images. Figure below shows an example performance of AO subsystem with our broad bandwidth light source and achromatizing lens.

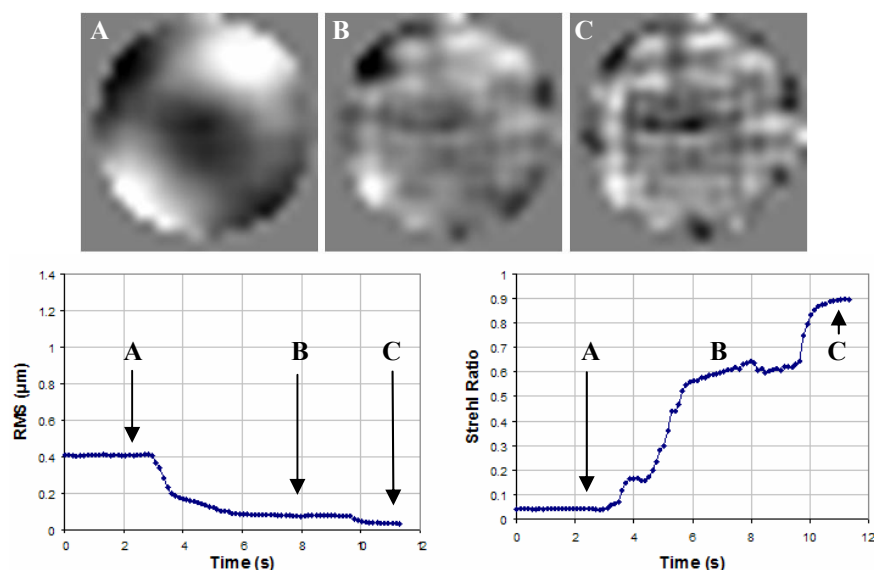


Fig. 3. Top: The ocular wavefront for T840-HP and achromatizing lens measured by the H-S wavefront sensor (A) before, (B) during DM1 and (C) during DM2 AO-correction. Bottom: plots shows total RMS wavefront error (left) and Strehl Ratio (right) during AO operation. The measurement times A, B, C from top panel are marked.

The pupil diameter of 6.7 mm used in our imaging system allows for up to 3 μm lateral resolution with good AO correction. To reduce head motion, a bite-bar and a forehead-rest assembly have been mounted on an X-Y-Z translation stage. This also allows precise positioning of the subject's eye. Eye fixation is directed to an external target to minimize head and eye motion and to allow precise imaging of different retinal locations. During the experiment, the subject's eye is dilated and cyclopleged by 1% Tropicamide and 2.5% Phenylephrine to ensure a pupil size > 7 mm and to paralyze accommodation. No trial lenses were used during testing (for all the subjects shown in this manuscript refractive error was within dynamic range of AO sub-system).

2.2. Acquisition of large FOV AO-OCT data sets

In order to improve clinical feasibility of our AO-OCT instrument we decided to provide large FOV hi-resolution retinal volumes rather than our current "small" volumes. In general in an AO-OCT instrument the size of the single volume is restricted by either of two factors: maximum lateral scanning area of the system or isoplanatic field of given eye. It practically means that maximum area covered by single AO-OCT volume (without compromising image resolution) is in the order of $2\text{-}3^\circ$ for our imaging wavelengths. In our previous work [7] we propose 1×1 mm 3D raster scanning mode that acquires 100 B-scans (1000 lines/B-scan) in about 5.5s (with line acquisition exposure of 50 μs) as most adequate for "large" AO-OCT Volume imaging. In this case volumetric sampling is not dense enough to see cellular structures; nevertheless it allows clear visualization of other interesting retinal features including micro capillaries and nerve fiber bundles. It's size however is still very small compared to the FOV of standard clinical instruments. Therefore we decided to use this scanning mode to acquire multiple volumes that could be use to create larger FOV AO-OCT volumes that would be of greater impact in clinical applications.

2.2.1. Acquisition of sub-volumes.

As mentioned above single AO-OCT sub-volume was set to cover about 1x1mm. It means that in case of large FOV sub-volume acquisition the spacing between centers of two consecutive sub-volumes should not exceed 70-80 % of sub-volume width i.e. 700-800 μm . This overlap of multiple sub-volumes is essential for later sub-volume co-registration and stitching. In order to change location of sub-volume we have been alternating location of fixation point that subject is looking at. This was the only way of changing location of sub volume since our single sub-volume uses whole scanning range of our instrument. Actually the only difference between this sub-volume acquisition and our regular data acquisition mode was the spacing between fixation points resulting in overlap in sub-volumes. As an example of AO-OCT scanning areas used in sub-volumetric measurements figure below shows 9 sub-volumes acquisition scheme.

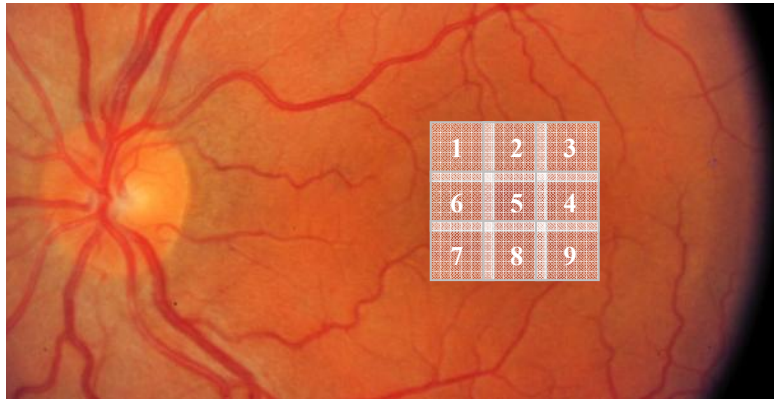


Fig. 4: An example of AO-OCT scanning areas used for large FOV creation (based on 9 sub-volumes acquisition). Numbers on the sub-volumes refer to the order in which they were acquired. Fundus photo is used for reference.

2.2.2. Stitching and Visualization of sub-volumes.

This new functionality (Stitching of sub-volumes) of our custom OCT Volume Renderer [16] will be described in details in our future reports. It basically allows active manipulation and viewing of the resulting volume and its cross sectional slices in real time. This feature allows overlaying of two volumes and manual co-registration based on position and structure of microcapillaries. In our current system we can translate freely volumes between each other in three dimensions. This data can be then stitched and saved as a single larger volume. This step is then repeated until large FOV volume consisting from all sub-volumes is created. On the areas where two volumes overlay we choose the maximum value of two overlaying Voxels as value of resulting Voxel. These large FOV data sets can then be manually co-registered to the fundus photo. This is possible due to another functionality of our OCT Volume Renderer, that allows active manipulation and viewing of fundus photo on corresponding OCT Volume, its OCT fundus and cross sectional slices. In our current system we can translate fundus photo freely in three dimensions. Additionally one can scale and rotate it along three main axes. All these manipulations are done with the fundus photo (OCT data remains unchanged). This approach allows keeping all the segmentations and annotation drawings done with OCT volume and allows it easy display on co-registered fundus photo.

2.3. Speckle reduction by multiple B-scan Averaging

As already mentioned in introduction speckles are inherently connected with OCT as a coherent detection scheme. However thanks to application of broadband light sources to AO-OCT system clear reduction in speckle size and therefore improvement in visibility of retinal features can be achieved. Unfortunately, beside clear improvement achieved by this method, its application to even greater reduction of speckle appearance (by increasing spectral bandwidth) is difficult to implement. This is mainly due to the high cost of broadband light sources and need for complex optical designs that would compensate for chromatic errors over larger spectral bands (not limited to longitudinal chromatic aberrations alone, but also compensating for eye transverse chromatic aberrations). To illustrate benefits of increased spectral bandwidth on AO-OCT images figure below shows comparison between two B-scans acquired with the same AO-OCT system over the same retinal location. The only difference between these two B-scans is spectral bandwidth of SLDs used for imaging. One image was acquired with our "old" SLD (50 nm @ 840nm with 6 μm axial resolution) second was acquired with new broadlighter SLD (112nm @ 836nm with 3 μm axial resolution).

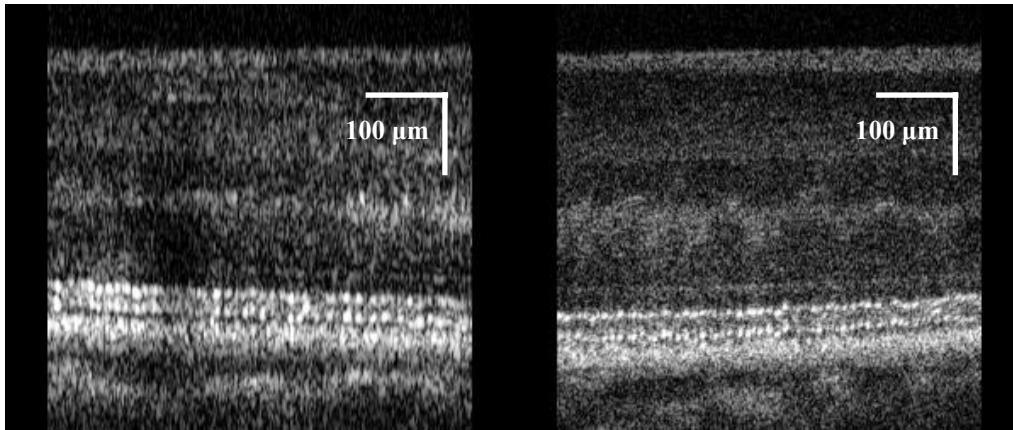


Fig. 5: B-scan acquired at 4.5° NR of the same subject by the 2DM's AO-OCT system with 6 μm (left) and 3 μm (right) axial resolution. AO focus was set on photoreceptor layers.

Another, already known way, of speckle contrast reduction includes averaging of multiple OCT B-scans. Unfortunately, with our current system acquisition speed, this method is not feasible for volumetric imaging and can be applied to the single location B-scans only. In our speckle reduction procedure presented in this paper we used an AO-OCT line scan that covers over 0.5 or 1mm retinal area. The acquisition speed equals 18 frames/s for 1mm and 36 frames/s for 0.5 mm scans. This data has been then post-processed what includes Frames registration [7]. In next step from set of 100 or 200 frames we choose 10 that has minimum motion artifacts and that show similar retinal structures (this is very important as vertical eye motion shifts our B-scans to different retinal locations). These frames are than averaged, each pixel value is calculated as an average intensity from all frames, to create one frame. An example result of this procedure is shown on figure below.

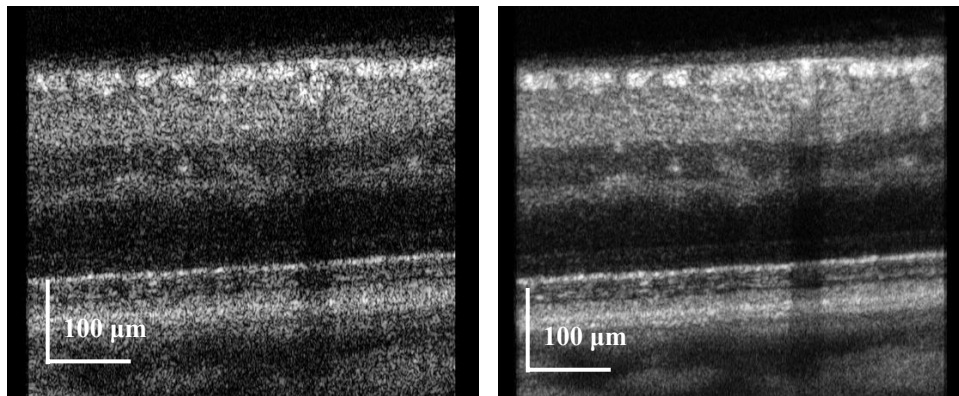


Fig. 6. UHR AO-OCT B-scan (0.5mm) Left: single Frame, Right: An average of 10 AO-OCT B-scan images. AO focus was set on inner retina layers.

In this case our AO sub-system was focused on inner retinal layers (increased sensitivity in RNFL). Clear reduction in speckle contrast can be observed between two images. Additionally contrast between NFL bundles and some capillaries is enhanced as well. Sever examples of implementing this method to images acquired on diseased retinal structures will be presented in result section of this manuscript.

3. RESULTS

As already mentioned in previous sections all the results presented in this paper has been acquired with ultra high resolution AO-OCT system constructed at UC Davis. AO correction was performed over 6.7 mm diameter of the subject's eye's pupil. For Fd-OCT data acquisition 50 μs line exposure time resulting in 18,000 lines/s acquisition speed. The results are divided into two subsections one focuses on large FOV volumetric AO-OCT imaging, other shows examples of speckle reduction on the single B-scans.

3.1. Volumetric Retinal imaging with AO-OCT

To visualize performance of our AO-OCT system an example of single AO-OCT sub-volume acquired over 1x1mm region on the retina is shown as a screen shot from our Volume Renderer.

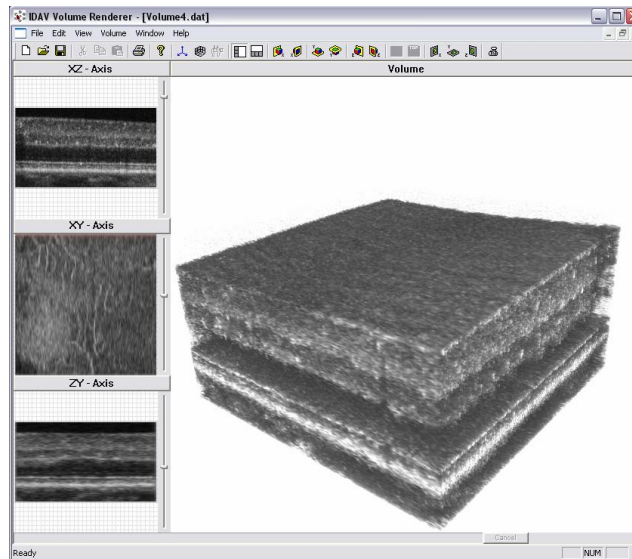


Fig. 7: An example visualization with Volume Renderer of AO-OCT 1x1mm volume acquired with focus set on inner retina layers.

It can be seen that even though vertical spacing between consecutive B-scans is in the order of 10 μ m microscopic retinal features can be easily visualized. As next example of volumetric imaging a Large FOV AO-OCT volume is presented. Figure 8. shows an OCT fundus view of 9 stitched sub-volumes with co-registered fundus photos. Registration of the sub-volumes and then co-registration between resulting Large FOV AO-OCT volume and fundus photo was done manually with our Volume Rendering software.

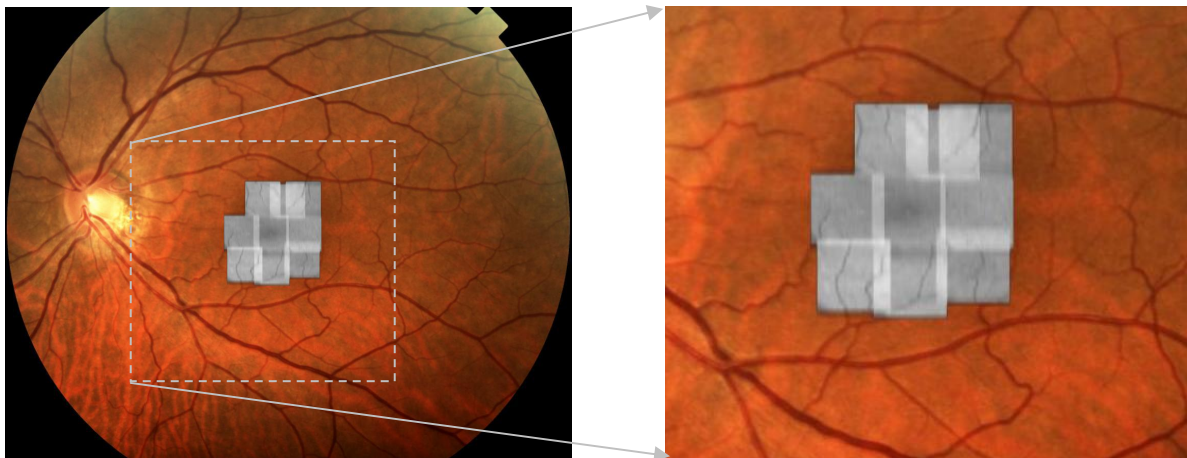


Fig. 8: An example visualization of OCT fundus created with our Volume Renderer of 9 stitched AO-OCT 1x1mm sub-volumes acquired with focus set on inner retina layers.

It can be seen that small retinal vessels can be used as marking points for co-registration of AO-OCT volumes to fundus photos. As results of this co-registration one can interactively view with our Volume Renderer both AO-OCT Volume and fundus photo that allows better visualization and localization of the retinal features between two imaging modalities. As an example of the volumetric view of large FOV AO-OCT volume figure below shows screen shot from our Volume Renderer.

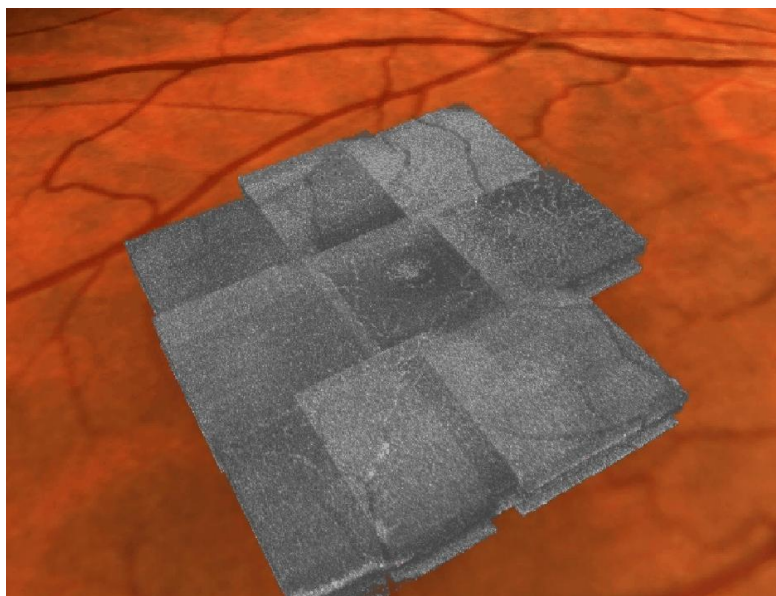


Fig. 9: An example visualization of the Large FOV AO-OCT Volume (from Fig. 8) with co-registered fundus photo.

We think that this feature, of creating and displaying large FOV OCT volumes, greatly improves clinical impact of our AO-OCT system. Especially when combined with more automated data acquisition and stitching procedures, that will be developed in the future.

3.2. Speckle reduction by multiple B-scan Averaging

In this section we will present three examples of AO-OCT image enhancing by applying multiple frames averaging. In all cases AO-OCT allowed better diagnosis of retinal conditions what was not possible with standard clinical imaging.

As first example figure below shows a single image and average one for subject with micro-scotoma located in the center of his visual field.

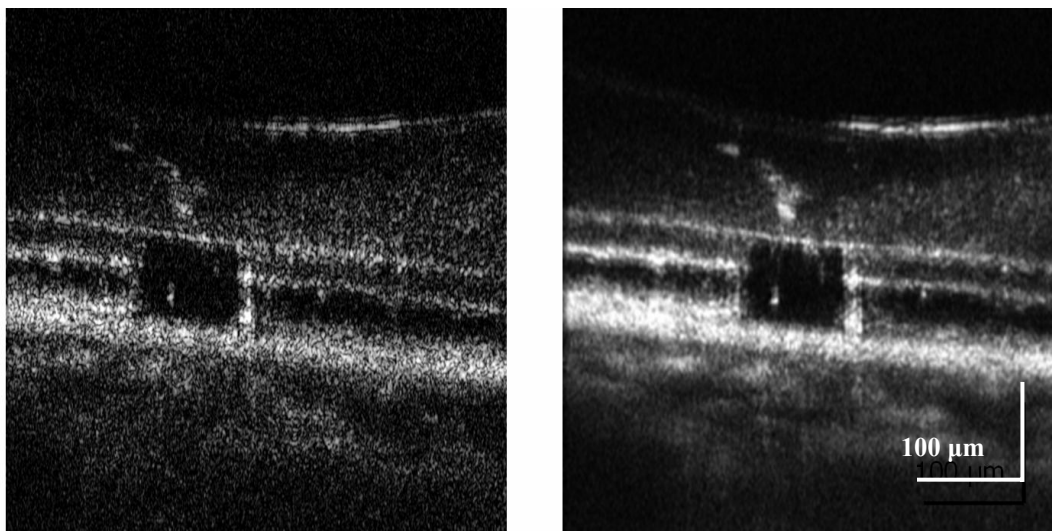


Fig. 10. UHR AO-OCT B-scan (0.5mm) acquired over center of the fovea. Left: single Frame, Right: An average of 10 AO-OCT B-scan images.

Please note that B-scan averaging allows clear reduction of speckle contrast. Additionally B-scans averaging increase system sensitivity (ability to see less reflecting structures). This is especially important in context of imaging diseased and elderly eyes which generally appears dimmer due to stronger absorption and scattering by ocular media.

Next example shown on figure below represent micro-traction in a center of the fovea that due to its size was not correctly diagnosed with other clinical imaging modalities (OCT, fundus photo).

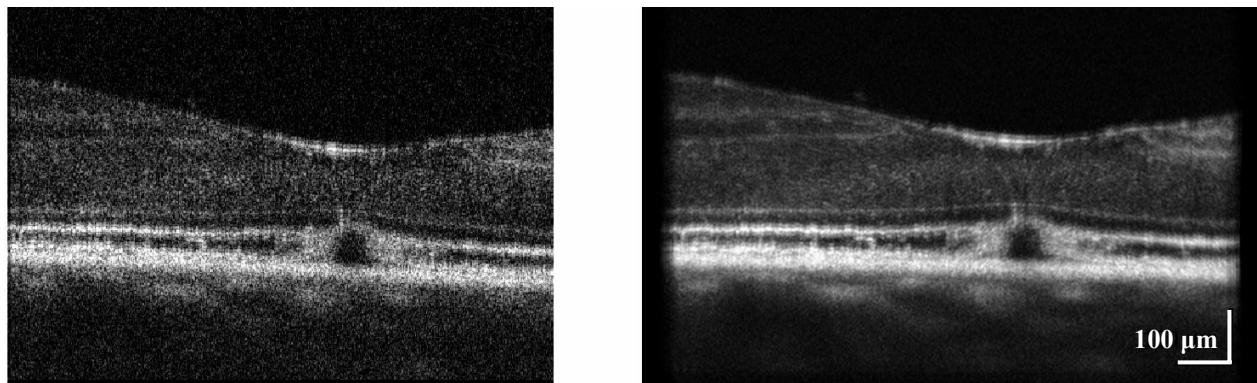


Fig. 11. UHR AO-OCT B-scan (1mm) acquired over center of the fovea. Left: single Frame, Right: An average of 10 AO-OCT B-scan images.

Here again clear improvement in speckle reduction and sensitivity can be observed, what allows inside into retinal structures on microscopic level.

Last example shown on figure 12 represents case of micro-scotoma that could not be explained by any standard imaging modality. It is evident however from AO-OCT B-scans that structural disruptions in outer nuclear layer translating to photoreceptor layers are good candidates to explain reduction in vision reported by this subject.

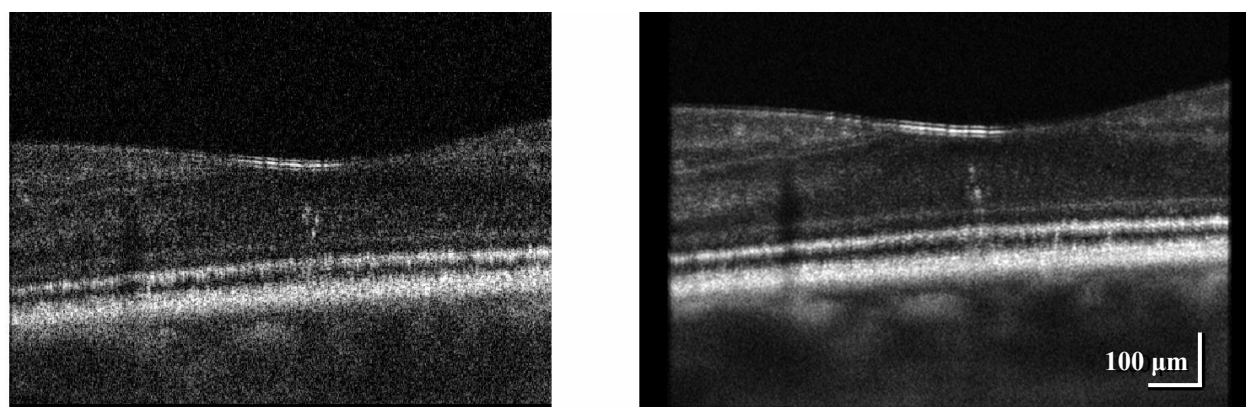


Fig. 12. UHR AO-OCT B-scan (1mm) acquired over center of the fovea. Left: single Frame, Right: An average of 10 AO-OCT B-scan images.

We think that these examples show that AO-OCT B-scans averaging may have an important role in displaying and diagnosing retinal diseases with AO-OCT instrumentation.

CONCLUSIONS

We presented our fully functional AO-OCT instrument that allows in-vivo imaging of retinal structures with $3\ \mu\text{m}$ volumetric resolution. Novel visualization methods presented in this manuscript include stitching of multiple sub-volumes to create large FOV AO-OCT volumes and co-registration of AO-OCT data to fundus photos. As result an interactive representation of AO-OCT Volume with corresponding fundus photo has been created. Additional simple method of B-scan averaging that resulted in reduction of the speckle contrast and enhancement of image sensitivity has been tested. As a result B-scans that are easier to interpret for clinicians have been created. We hope that both methods help to popularize AO-OCT as a clinically relevant imaging modality.

ACKNOWLEDGEMENTS

We gratefully acknowledge the contributions of Joseph A. Izatt from the Department of Biomedical Engineering, Duke University Durham, NC. The help of Alfred R. Fuller, David F. Wiley, and Bernd Hamann from the Institute for Data Analysis and Visualization (IDAV), UC Davis for developing 3D visualization software and Bioptigen Inc. Durham, NC for providing OCT data acquisition software is appreciated. This research was supported by the National Eye Institute (EY 014743).

REFERENCES

1. D.T. Miller, J. Qu, R.S. Jonnal, and K. Thorn, "Coherence gating and adaptive optics in the eye" in Coherence Domain Optical Methods and Optical Coherence Tomography in Biomedicine VII, Valery V. Tuchin, Joseph A. Izatt, James G. Fujimoto, Proc. SPIE 4956, 65-72 (2003)
2. B. Hermann, E.J. Fernandez, A. Unterhubner, H. Sattmann, A.F. Fercher, and W. Drexler, P.M. Prieto and P. Artal, "Adaptive-optics ultrahigh-resolution optical coherence tomography", Opt. Lett. **29**, 2142-2144 (2004)
3. Y. Zhang, J. Rha, R. Jonnal, and D. Miller, "Adaptive optics parallel spectral domain optical coherence tomography for imaging the living retina," Opt. Express **13**, 4792-4811 (2005)
4. E. Fernández, B. Povazay, B. Hermann, A. Unterhuber, H. Sattman, P. Prieto, R. Leitgeb, P. Anhalt, P. Artal, W. Drexler, "Three-dimensional adaptive optics ultrahigh-resolution optical coherence tomography using liquid crystal spatial light modulator" Vis. Research **45**, 3432-3444 (2005)
5. R.J. Zawadzki, S. Jones, S. Olivier, M. Zhao, B. Bower, J. Izatt, S. Choi, S. Laut, and J. Werner, "Adaptive-optics optical coherence tomography for high-resolution and high-speed 3D retinal in vivo imaging," Opt. Express **13**, 8532-8546 (2005)
6. Y. Zhang, B. Cense, J. Rha, R. S. Jonnal, W. Gao, R. J. Zawadzki, J. S. Werner, S. Jones, S. Olivier, and D. T. Miller, "High-speed volumetric imaging of cone photoreceptors with adaptive optics spectral-domain optical coherence tomography," Opt. Express **14**, 4380-4394 (2006)
7. R.J. Zawadzki, S.S. Choi, S.M. Jones, S.S. Oliver, and J.S. Werner, "Adaptive optics-optical coherence tomography: optimizing visualization of microscopic retinal structures in three dimensions," J. Opt. Soc. Am. A **24**, 1373-1383 (2007)
8. C.E. Bigelow, N.V. Iftimia, R.D. Ferguson, T.E. Ustun, B. Bloom, and D.X. Hammer, "Compact multimodal adaptive-optics spectral-domain optical coherence tomography instrument for retinal imaging," J. Opt. Soc. Am. A **24**, 1327-1336 (2007)
9. A.F. Fercher, C.K. Hitzenberger, G. Kamp, Y. Elzaiat, "Measurement of intraocular distances by backscattering spectral interferometry", Opt. Commun. **117**, 43-48 (1995)
10. M. Wojtkowski, T. Bajraszewski, P. Targowski and A. Kowalczyk "Real time in vivo imaging by high-speed spectral optical coherence tomography", Opt. Lett. **28**, 1745-1747 (2003)
11. N.A. Nassif, B. Cense, B.H. Park, M.C. Pierce, S.H. Yun, B.E. Bouma, G.J. Tearney, t.C. Chen, J.F. de Boer "In vivo high-resolution video-rate spectral-domain optical coherence tomography of the human retina and optic nerve", Opt. Express **12**, 367-376 (2004)
12. R.J. Zawadzki, Y. Zhang, S.M. Jones, R.D.Ferguson, S.S. Choi, B. Cense, J.W. Evans, D. Chen, D.T. Miller, S.S. Olivier, J.S. Werner, "Ultrahigh-resolution adaptive optics - optical coherence tomography: toward isotropic 3 μ m resolution for in vivo retinal imaging", BIOS 2007 Proc. SPIE Vol. 6429, (2007)
13. E. Fernández, A. Unterhuber, P. Prieto, B. Hermann, W. Drexler, and P. Artal, "Ocular aberrations as a function of wavelength in the near infrared measured with a femtosecond laser," Opt. Express **13**, 400-409 (2005)
14. E. Fernández and W. Drexler, "Influence of ocular chromatic aberration and pupil size on transverse resolution in ophthalmic adaptive optics optical coherence tomography," Opt. Express **13**, 8184-8197 (2005)
15. E. Fernández, L. Vabre, B. Hermann, A. Unterhubner, B. Povezay, W. Drexler, "Adaptive optics with a magnetic deformable mirror: applications in the human eye", Opt. Express **14**, 8900-8917 (2006)
16. R.J. Zawadzki, A.R. Fuller, D.F. Wiley, B. Hamann, S.S. Choi, J.S. Werner, "Adaptation of a support vector machine algorithm for segmentation and visualization of retinal structures in volumetric optical coherence tomography data sets," Journal of Biomedical Optics **12**, 041206 (1-8) (2007)